applied sciences

MDPI

Article

Bedding Slope Destabilization under Rainfall: A Case Study of Zhuquedong Slope in Hunan Province, China

Fan Xu [1,2], Huihua Hu [1,3], Hang Lin [1,2,4,*] and Linglin Xie [2,4]

[1] School of Resources and Safety Engineering, Central South University, Changsha 410083, China; csu_xufan@163.com (F.X.); huhuihuahnjg@126.com (H.H.)
[2] Key Laboratory of Natural Resources Monitoring and Supervision in Southern Hilly Region, Ministry of Natural Resources, Changsha 430071, China; xielinglincs@126.com
[3] Hunan Provincial Communications Planning, Survey and Design Institute, Changsha 410200, China
[4] The Second Surveying and Mapping Institute of Hunan Province, Changsha 430071, China
* Correspondence: hanglin@csu.edu.cn

Abstract: The soft interlayer and rock structure play a significant role in controlling the deformation of the bedding slope, and it is necessary to consider the phenomenon of the sudden change of local response in these key parts under rainfall conditions, and then to clarify the mechanism of rainfall infiltration and damage mechanism of such slopes. In this paper, a large red-layered flat-dipping bedding landslide was selected as the research object, and numerical calculations based on the Van Genuchten model for saturated–unsaturated flow were performed in order to investigate the hydrological response and distribution patterns of water within the slope during rainfall. Moreover, stability analysis was performed based on the seepage field results and secondary development of FLAC^{3D}, and the landslide evolution process was simulated and reproduced using the constitutive model of double-variables and the strength reduction method (SRM). The results showed that the effects of heavy rainfall on the water distribution and stability of the highway slope are significant, while the effects on the natural slope are not significant. There are three phases of the slope destabilization: flexure and uplift state, deformation exacerbation state and shear failure state. The slope destabilization mechanism is a typical "sliding-bending-shearing" type. The results of the study can provide a theoretical basis for the study of the seepage, stability analysis and destabilization mechanism of bedding slopes.

Keywords: bedding slope; rainfall; seepage; stability analysis; destabilization mechanism

check for updates

Citation: Xu, F.; Hu, H.; Lin, H.; Xie, L. Bedding Slope Destabilization under Rainfall: A Case Study of Zhuquedong Slope in Hunan Province, China. *Appl. Sci.* **2024**, *14*, 1394. https://doi.org/10.3390/app14041394

Academic Editor: Tiago Miranda

Received: 17 January 2024
Revised: 6 February 2024
Accepted: 6 February 2024
Published: 8 February 2024

Copyright: © 2024 by the authors. Licensee MDPI, Basel, Switzerland. This article is an open access article distributed under the terms and conditions of the Creative Commons Attribution (CC BY) license (https://creativecommons.org/licenses/by/4.0/).

1. Introduction

China is a country where geological hazards are extremely frequent, with landslide hazards accounting for nearly half of them. The contradiction between the rapidly growing population and the limited urban space has led to the advancement of the scope of human life and engineering activities to remote areas, and engineering activities such as road, bridge and tunnel construction are increasingly carried out in mountainous areas [1,2]. As a common slope type in mountainous areas, flat-dipping bedding slopes are widely distributed in China and present many stability problems, among which rainfall-induced landslides are widespread and frequent [3–5]. The economic losses caused by bedding landslides under rainfall conditions are huge, which has become a key problem to be solved in engineering construction and operation in mountainous areas.

The study of slope seepage under rainfall conditions is the basis of stability studies; combining hydraulic modeling and examples of slopes, the water distribution and migration patterns within the slopes were studied. Kacimov et al. [6] studied reservoir bank slopes under rainfall conditions and found that the water evaporation from the slopes is characterized by uniform spatial distribution and variation with time. Qi et al. [7] discussed the mathematical model of rainfall infiltration on rocky slopes, and analyzed the variation

of matrix suction and the development of the transient saturation zone. In terms of indoor experiments, Huat et al. [8] studied the effects of slope angle and surface cover on the infiltration water volume and matrix suction, and found that the infiltration rate is low when the surface is covered with grass or geosynthetic mesh, and the infiltration water volume decreases with the increase in slope angle. Chen et al. [9] used model tests to analyze the response process of pore water pressure within the slope under rainfall conditions, and divided the response process into slow-change phase, surge phase and stable phase. However, the presence of structural surfaces for bedding slope containing weak interlayers makes the seepage field within the slope complex and variable, which is not well resolved.

Combined with the research results of slope seepage under rainfall conditions, scholars conducted in-depth research on slope stability under rainfall conditions. In terms of theoretical analysis, Lian et al. [10] combined the Mohr–Coulomb theory to calculate infinitely long soil slopes under seepage parallel-to-slope surface conditions, and analyzed the soil rupture surface with logarithmic helix morphological characteristics using the definite integral element method. Conte et al. [11] proposed a method of practical interest for predicting shallow landslide triggering due to expected rainfall scenarios, which depends on basic parameters such as slope geometry and soil properties. In terms of numerical simulation, Liu and Zhou [12] proposed an unsaturated hydraulic stress coupling model based on the DDA method and found that the difference of slope stability coefficients, with or without considering hydraulic coupling, is related to the rainfall intensity. Due to the complexity of rainfall-induced changes in the seepage and stress fields of slopes, most studies only considered slopes with simple geological conditions or used statistical methods [13,14]. In general, the principle of rainfall-induced slope instability is summarized as follows: rainwater softens the mudstone and reduces matric suction in the soil, and changes in physical and mechanical properties lead to a reduction in slip resistance [15]. Under the joint action of rainwater equivalent load and slope property change, the sliding force of the rock–soil body on the slip surface is greater than the sliding resistance force, and the slope is destabilized and damaged.

However, abundant engineering practice showed that soft interlayer and rock structure play a significant role in controlling the deformation of bedding slopes [16]. In order to clarify the mechanism of rainfall infiltration and the damage mechanism of such slopes, this paper selected a large flat-dipping bedding landslide as the research object, and used finite element analysis of the rainfall infiltration process of the slope based on the Van Genuchten model to study the spatial distribution patterns of volumetric water content and pore water pressure within the slope. Combined with the results of seepage field analysis, the slope stability analysis was carried out by the strength reduction method, and the finite difference method was applied to calculate and reveal the deformation and failure modes of the slope.

2. Engineering Background

The Zhuquedong landslide is located in Luxi County, Hunan Province, China (Figure 1a), and belongs to the hilly area of tectonic denudation, with an elevation of 282 m at the top of the slope and about 125 m at the foot of the slope, and a slope gradient of 10°–20°. The slope body is basically a bedding slope, forming a stepped slope topography with orange groves, paddy fields and vegetable fields. The dip angle of the slope ranges from 14° to 30°, which shows the trend that the dip of the rock layer from the trailing edge to the front edge gradually changes from steep to gentle. The perimeter of the landslide is in the shape of a circle chair (Figure 1b,c), which is mainly controlled by the structure. The length of the landslide is 448 m along the direction perpendicular to Changji Road, the width is 425 m along Changji Road, and the width of the front edge at the foot of the slope is about 500 m.

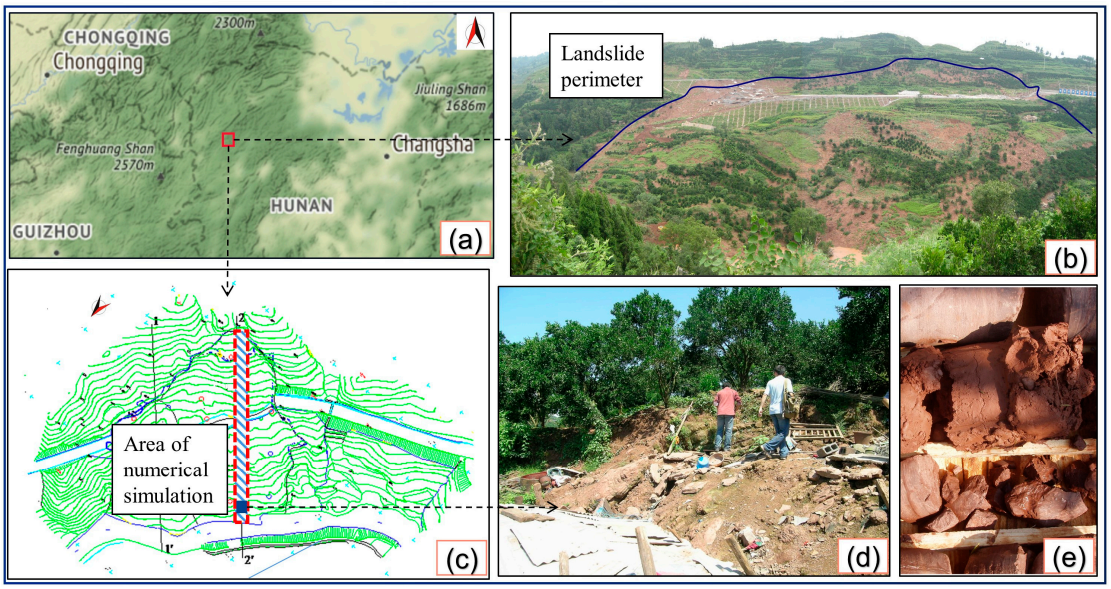


Figure 1. Location of study region: (**a**) geographic location; (**b**) sliding boundary; (**c**) landslide shape; (**d**) a ridge of creeping bend in the lower reaches; (**e**) siltized intercalation.

The landslide is located in the red layer area where a large number of geological hazards occur. Mudstone, siltstone and other soft rocks with weak permeability and strong hydrophilicity are more abundant in the red layer, which have the characteristics of easy softening with water, easy disintegration with water loss and low strength. The soft interlayer formed by water softening of mudstone and the interlayer misalignment zone in the red layer rock body largely controls the deformation and damage mode of the rock body [10]. Therefore, red-layered mudstone slope instability is characterized by strong suddenness and difficulty in early identification. The field survey results show that the upper part of the Zhuquedong slope is covered by the Quaternary System, and the surface layer exposed is mainly fill soil, planting soil distributed in farmland, sub-clay and block gravel, etc. The underlying rocks are mainly silty mudstone and calcareous sandstone, and decomposed rocks and soft interlayer are revealed during the survey. The silty mudstone of the strongly weathered layer is relatively broken, the core is gravelly and fragmented, and the lithology is relatively soft. Weakly weathered silty mudstone is soft and relatively intact, which is enormously easy to be softened by water to form soft interlayer (Figure 1e), with an interlayer misalignment zone existing locally. Slightly weathered calcareous sandstone is hard and relatively intact. Sliding zone soils are mainly the soft interlayer and mudification interlayer formed by silty mudstone and the interstratigraphic misalignment zone after water softening, which is about 0.5–2 m thick.

The landslide toe is located at the foot of the slope, and part of the rock–soil body washes into the Danqing River. The sliding surface (belt) attitude of the slope body is controlled by the attitude of bedrock. The dip angle of the slide surface (belt) is steep in the trailing and slow in the front, with the dip angle of the trailing edge about 21–30° and the dip angle of the front edge about 14–17°. The shape of the sliding surface is controlled by the rock strata, and also by the influence of steeply dipping joints, so the sliding surface is locally stepped. The slide surface develops landslide scrapes, and its slip direction is consistent with the main slide direction. The lower slide bed lithology of the sliding surface is mainly relatively intact weakly and slightly weathered rocks. The landslide mass is mainly composed of residual gravelly soil—strongly and weakly weathered rocks, with a slide thickness of about 0–20 m and a sliding volume of about 2.6 million m^3. Landslide uplift and depressions appear together, mainly near the front edge of the slope; the front end of the depression is uplift; the local presence of the uplift is the trap pit; and the formation of the uplift is affected by the sliding and bending deformation of the rock

layer (Figure 1d). The cracks in the landslide mass can be divided into tension cracks and bulging cracks according to the mechanical properties. Affected by the high-speed slip, some landslide mass in the front has been dismembered into loose bodies, and the landslide cracks are relatively clear at the boundary and bulging mound.

The surface water catchment area of the landslide area is large, and atmospheric precipitation is the main source of groundwater and surface water. The surface water mainly exists in the Danqing River, which flows from north to south through the about 900 m long foot of the slope, forming an obvious U-shaped bend, and the mountain is located on the scouring bank of the river bend. The river level is greatly influenced by atmospheric precipitation, which rises abruptly during the rainy season. Before the occurrence of landslide, the elevation of Danqing River bed was about 124–125 m, and the foot of the slope near the river was a steep terrain. After the landslide occurred, the front edge of the slide washed into the Danqing River, causing the river to be blocked to form a weir. After dredging the river, the riverbed height was raised to 127–130 m.

3. Theoretical Model of Slope Seepage and Stability under Rainfall Conditions

3.1. Seepage Theory

The calculation of rainfall infiltration considering the unsaturated zone can better reflect the actual situation. The differential equation for saturated–unsaturated seepage in a homogeneous isotropic medium expressed by the improved Darcy's law is as follows:

$$\frac{\partial}{\partial x}\left(k_{\mathrm{u}}\frac{\partial h_p}{\partial x}\right)+\frac{\partial}{\partial y}\left(k_{\mathrm{u}}\frac{\partial h_p}{\partial y}\right)+\frac{\partial}{\partial z}\left(k_{\mathrm{u}}\frac{\partial h_p}{\partial z}\right)+\frac{\partial k_{\mathrm{u}}}{\partial z}=\left[C\left(h_p\right)+\beta S_{\mathrm{s}}\right]\frac{\partial h_p}{\partial t} \tag{1}$$

$$k_{\mathrm{u}}=k_{\mathrm{s}}k_{\mathrm{r}}\left(h_p\right) \tag{2}$$

$$S_{\mathrm{s}}=\rho_{\mathrm{w}}g(\alpha_{\mathrm{r}}+\phi\alpha_{\mathrm{w}}) \tag{3}$$

where k_{u} is the unsaturated hydraulic conductivity (m/s); k_{s} is the saturated hydraulic conductivity (m/s); k_{r} is the relative permeability; h_{p} is the pressure head (m); C is the water capacity (−); S_{s} is the specific storage (m^{-1}), for unsaturated media, S_{s} = 0; β is the selection parameter (−) with saturated region β = 1 and unsaturated region β = 0; α_{r} is the compressibility of rock (−); α_{w} is the compressibility of water (−); ϕ is the porosity (−); and ρ_{w} is the density of water ($\mathrm{kg/m}^3$).

The water content curve (moisture characteristic curve) of the material expresses the relationship between the volumetric water content θ and the matrix suction ψ. Numerous experiments and numerical simulations [17,18] showed that the classical Van Genuchten model with appropriate parameters is suitable for representing the water content relationship in unsaturated fractured rocks and soils, and accordingly, accurate seepage field results are beneficial for slope stability analysis, expressed as

$$S_{\mathrm{e}}=\frac{\theta-\theta_{\mathrm{r}}}{\theta_{\mathrm{s}}-\theta_{\mathrm{r}}}=\left[\frac{1}{1+(\alpha\psi)^n}\right]^m \tag{4}$$

where S_{e} is the effective saturation (−); θ_{s} is the saturated volumetric water content (−); θ_{r} is the residual volumetric water content (−); and α, n and m are empirical parameters indicating the shape of the soil moisture characteristic curve with $m = 1 - 1/n$.

The permeability function ($k_{\mathrm{u}} - \psi$ equation) of the material is related to the relationship of $\theta - k_r$. The moisture characteristic curve is brought into the Mualem [19] conceptual model to calculate k_{r}:

$$k_{\mathrm{r}}=S_{\mathrm{e}}^{1/2}\left[1-\left(1-S_{\mathrm{e}}^{1/m}\right)^m\right]^2 \tag{5}$$

Combining Equations (4) and (5), the permeability function of the material can be obtained.

3.2. Slope Stability Theory

The double-variables strength theory proposed by Fredlund and Rahardjo [20] is used to describe the shear strength of fractured rocks and soils:

$$\tau_f = c' + (\sigma_n - \mu_a)\tan\varphi' + (\mu_a - \mu_w)\tan\varphi^b \quad (6)$$

where τ_f is the shear strength of unsaturated material (kPa); c' is the effective cohesion (kPa); σ_n is the effective normal stress (kPa); u_a is the pore air pressure (kPa); u_w is the pore water pressure (kPa); φ' is the effective friction angle (°); φ^b is the suction internal friction angle (°); and $\mu_a - \mu_w$ is the matrix suction (kPa). Without considering the matrix suction or when the material is close to saturation, $(\mu_a - \mu_w)\tan\varphi^b = 0$, and Equation (6) is the formula for saturated materials.

The rock–soil body is assumed to be ideal elastic-plastic bodies, and the constitutive model of the double-variables strength theory is used [21]. Based on SRM [22], the shear strength of the material is reduced when the three shear strength parameters are simultaneously divided by an increasing reduction factor until the slope is in a state of instability and failure [23]:

$$\frac{\tau_f}{SRF} = \frac{c'}{SRF_{c'}} + (\sigma_n - u_a)\frac{\tan\varphi'}{SRF_{\varphi'}} + \chi(u_a - u_w)\frac{\tan\varphi^b}{SRF_{\varphi^b}} \quad (7)$$

where SRF is the strength reduction factor—the slope is critically unstable with $SRF = FOS$; $SRF_{c'}$, $SRF_{\varphi'}$, SRF_{φ^b} are the reduction factors of effective cohesion, effective friction angle and suction internal friction angle, respectively; and χ is the empirical coefficient.

It is usually assumed that $SRF_{c'} = SRF_{\varphi'} = SRF_{\varphi^b} = SRF$. Combined with Equation (7), the shear strength parameters of the rock–soil body when the slope is in ultimate equilibrium can be obtained as follows:

$$\begin{cases} c'_F = \frac{c'}{FOS} \\ \varphi'_F = \arctan\left(\frac{\tan\varphi'}{FOS}\right) \\ \varphi^b_F = \arctan\left(\frac{\tan\varphi^b}{FOS}\right) \end{cases} \quad (8)$$

4. Numerical Model of Bedding Slope

4.1. Parameterization

The shear strength parameters of the rock–soil body were obtained by drilling the in situ samples of landslide mass for the indoor large-scale direct shear test, combined with the physical exploration technology. The VG model parameters of the rock–soil body are determined by combining the characteristics of this project and similar projects [24], and the hydraulic parameters and mechanical parameters are presented in Table 1.

Combining the above VG-M theoretical model and parameters, the soil–water characteristic curves and the permeability functions ($k_u - \psi$ equation) of the material are calculated, as shown in Figure 2.

Based on the data of Jishou ground meteorological station in Hunan Province, the meteorological conditions of the Zhuquedong landslide were summarized and the rainfall observation data were analyzed; the variation of rain intensity with time is shown in Figure 3. The rainfall in July 2007 was the maximum of the year in the area, with 98.2 mm of cumulative rainfall from the 10th to the 14th, and 229.3 mm of cumulative rainfall from the 21st to the 26th. In total, there were five days with daily rainfall exceeding the heavy rainfall standard and four times with daily rainfall exceeding the torrential rainfall standard.

Table 1. Summary of parameters.

Symbol	Parameter Name	Units	Sub-Clay/Fill Soil	Strongly Weathered Silty Mudstone	Weakly Weathered Silty Mudstone	Soft Interlayer	Slightly Weathered Calcareous Sandstone
θ_s	Saturated water content	(–)	0.3	0.3	0.2	0.3	0.1
θ_r	Residual water content	(–)	0.05	0.05	0.03	0.05	0.02
k_s	Saturated hydraulic conductivity	(m/s)	1×10^{-6}	1×10^{-6}	5×10^{-4}	1×10^{-6}	1×10^{-5}
α	Van Genuchten fitting parameter	(kPa)	100	1	0.5	10	0.2
n	Van Genuchten fitting parameter	(–)	1.5	1.5	2	1.5	5
E	Young's modulus	(MPa)	10	1000	1500	20	1×10^4
v	Poisson's ratio	(–)	0.35	0.3	0.25	0.35	0.15
c'	Effective cohesion	(kPa)	10	25	27	6	390
φ'	Effective friction angle	(°)	14	19	24	12	40
φ^b	Suction internal friction angle	(°)	14	14	14	14	14
ρ	Density	(kg/m^3)	1900	2430	2500	1920	2600

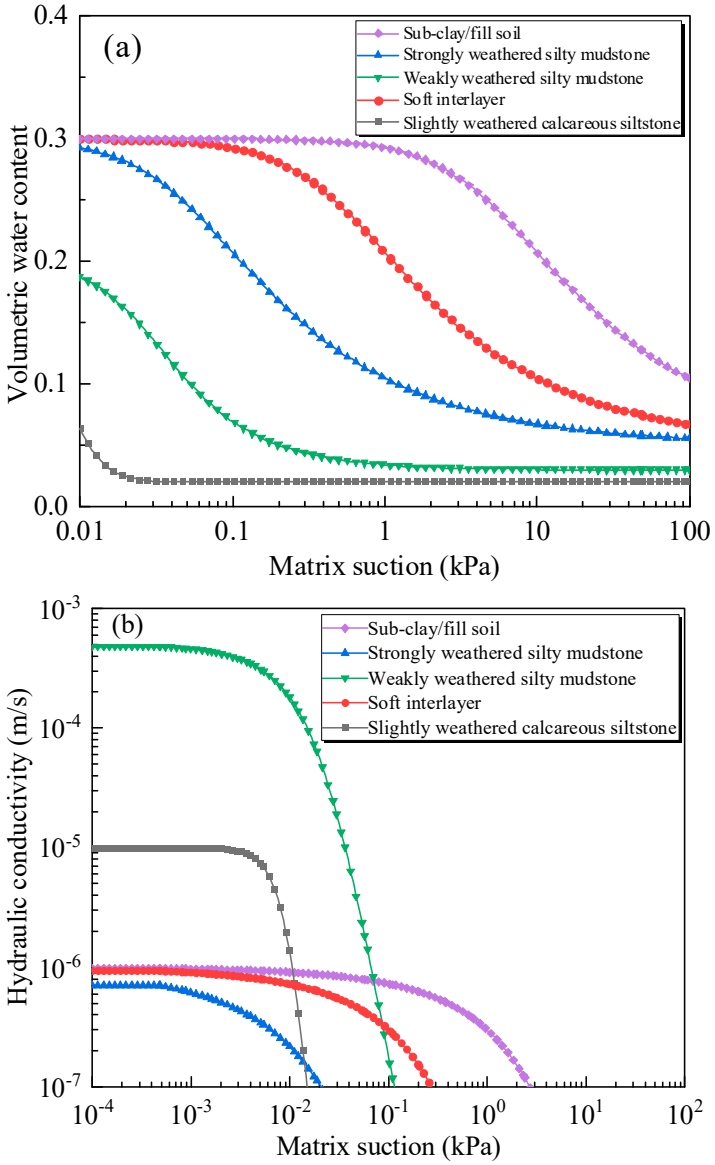


Figure 2. (**a**) Soil–water characteristic curves; (**b**) Permeability functions for different materials zones.

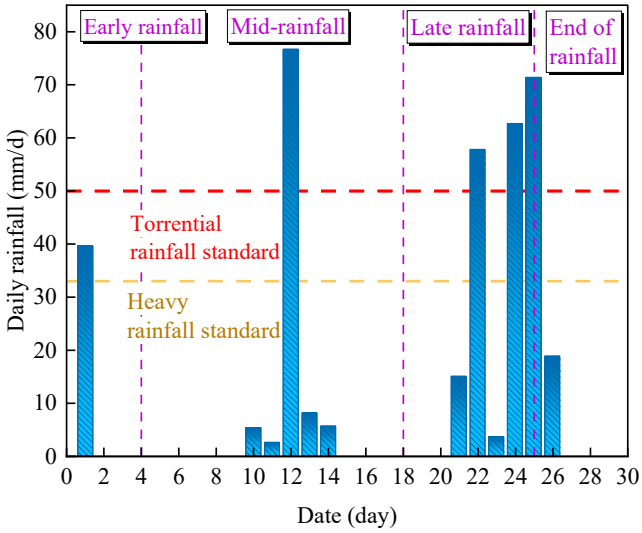


Figure 3. Rainfall monitoring data.

4.2. Numerical Modeling

The slope height is 164 m, and the length is 536 m. The whole model is defined as a series of geometric objects, and the type of zone is given as quadrilateral and triangle. The global zone size is 5 m, with the local mesh encryption carried out for the surface and interlayer. The post-excavation (highway) slope model has a total of 2497 nodes and 2382 zones, and the pre-excavation (natural) slope model has a total of 2512 nodes and 2396 zones. The numerical calculation model of the slope and its boundary conditions is shown in Figure 4a,b. For seepage calculations, the left and right boundaries below the initial water table are set as boundaries of the constant water head, with the hydraulic head of 136 m and 29.5 m, respectively. Moreover, the left and right boundaries above the initial water table and the bottom boundary are set as impermeable boundaries. The surface of the slope is the rainfall infiltration boundary and set as the flow boundary. The rainfall infiltration boundary needs to be considered in relation to the magnitude of the rainfall intensity and the infiltration capacity of the topsoil: when the rainfall intensity is less than the infiltration capacity of the topsoil, it is treated as the flow boundary condition; when the rainfall intensity is stronger than the infiltration capacity of the topsoil, part of the rainfall forms overland runoff, and the boundary is treated as the boundary of the fixed water level. For stress and strain calculations, the left and right boundaries are constrained in the horizontal direction, and the bottom boundary is fixed in all directions.

Because the modeling conditions and influencing factors of Zhuquedong slope are complex and the theoretical analysis is difficult to apply directly, the finite-difference numerical software FLAC^{3D} 6.0 is used to analyze the evolution process and damage mechanism of the whole process of the slope. When FLAC^{3D} software performs seepage analysis, it automatically adjusts the negative pore water pressure to zero and is unable to determine the hydraulic conductivity based on the saturated state of the geotechnical body [25]. In this paper, we choose to import the finite element seepage calculation results of saturated–unsaturated slope geotechnical bodies into FLAC^{3D}, which mainly considers two main effects of rainfall infiltration on the slope.

(1) Rainwater has a deteriorating effect on geotechnical bodies and reduces their shear strength [26]. For this purpose, the strength decay function of the geotechnical body is constructed through the FISH language, as in Equations (9) and (10), where $c(\mu_w)$ is the integrated cohesion value related to the pore water pressure, and in general, $c(\mu_w)$ decreases with the increase in pore water pressure. Based on the pore water pressure value of each node obtained by traversing, the attenuated geotechnical body shear strength value is

calculated and assigned to the zones according to the spatial coordinates, as shown in Figure 5.

$$\tau_f = c(\mu_w) + (\sigma_n - \mu_a)_f \tan \varphi' \quad (9)$$

$$c(\mu_w) = c' + \chi(\mu_a - \mu_w)_f \tan \varphi^b \quad (10)$$

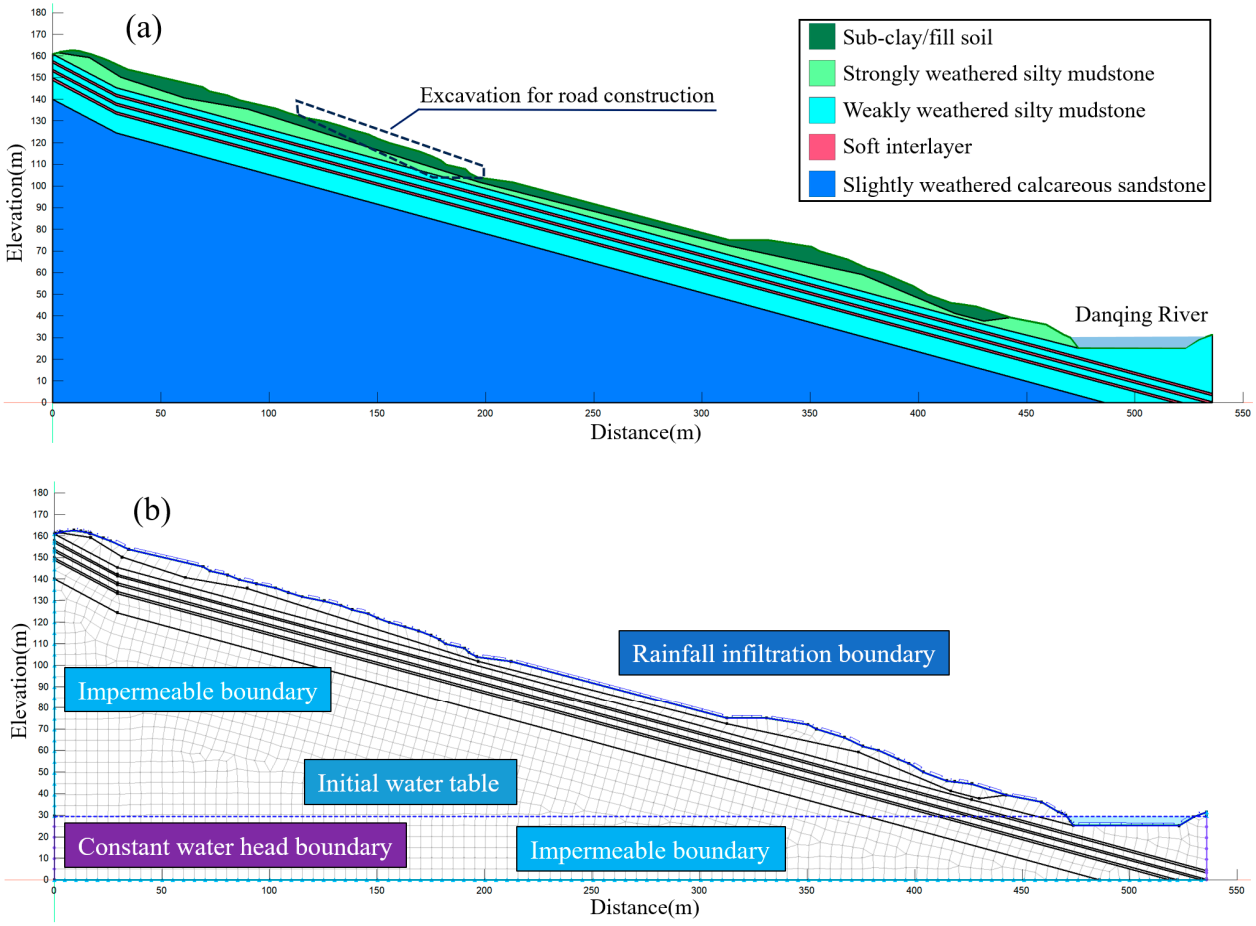


Figure 4. Numerical model of Zhuquedong slope: (**a**) hydrogeological profile; (**b**) mesh generation and boundary conditions.

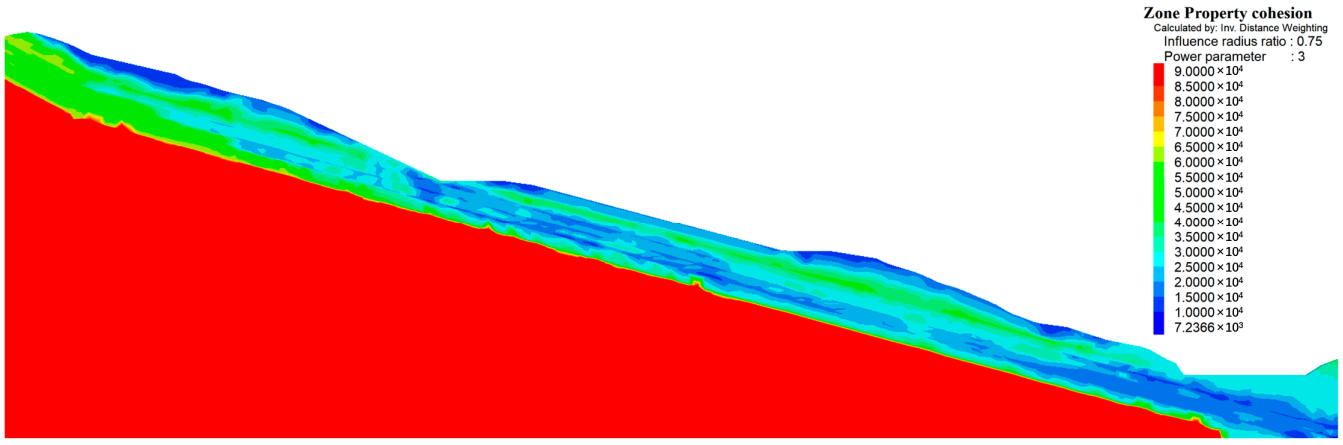


Figure 5. Slope cohesion distribution after strength decay.

(2) The infiltration and recharge of rainwater increases the pore water pressure in the slope, and the presence of buoyancy forces reduces the pressure between the rock layers,

which reduces the slip resistance of the slip surface and leads to shear damage, and rupture of the top of the slope occurs when the buoyancy force is too large [27]. For this purpose, the pore water pressure values at each node are traversed and determined to be positive or negative through the FISH language, and the positive values are applied to the nodes of the slope model according to the spatial coordinates, as shown in Figure 6.

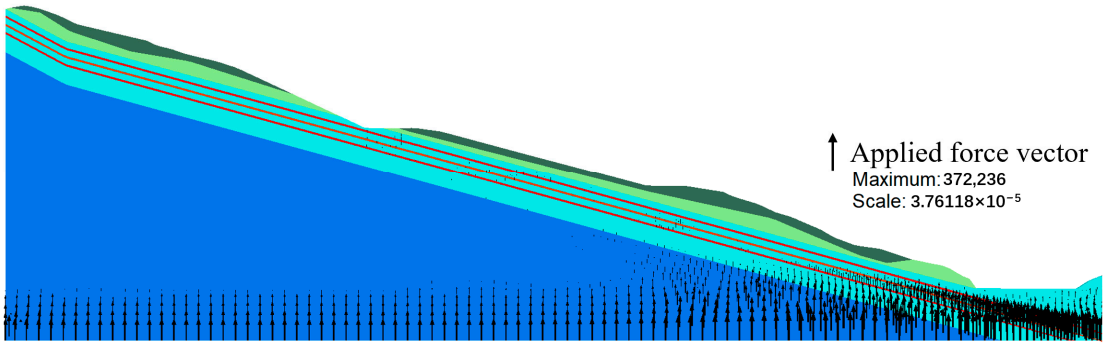


Figure 6. Water pressure distribution in the slope.

After solving the problem of rainfall infiltration on the slope in FLAC^{3D}, the zones are modeled with the Mohr–Coulomb criterion, which allows for normal iterative computation [28]. Finally, the slope unit flow and pore water pressure distribution are derived for seepage analysis, and the deformation and the factor of safety (*F*s) results are derived for slope evolution process and stability analysis, and the process is shown in Figure 7.

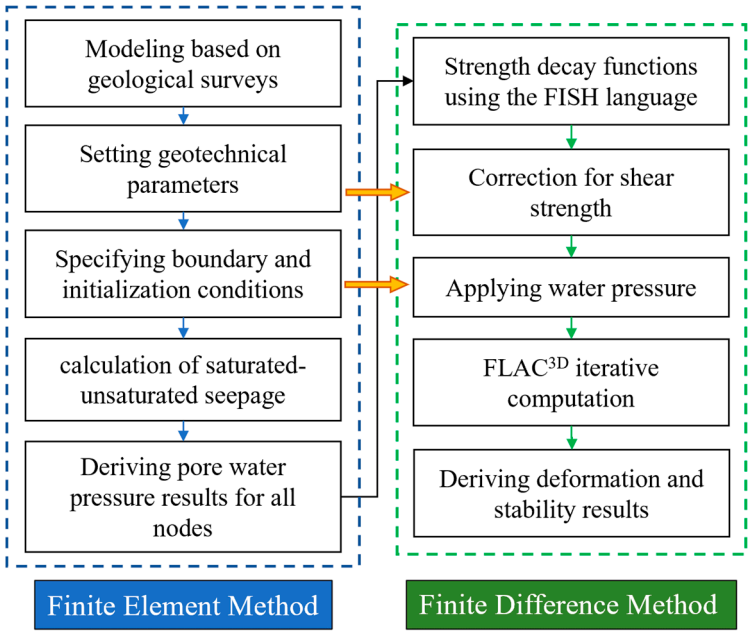


Figure 7. Slope seepage-deformation calculation process.

4.3. Analysis of Seepage Results

4.3.1. Highway Slope Seepage Analysis

In order to obtain the initial conditions of flow, geotechnical saturation and pore water pressure inside the slope at the beginning of the calculation, the highway slope is pre-analyzed and processed for 30 days under no-rainfall conditions. The initial state of the slope is shown in Figures 8a and 9a, where there is essentially no flow within the slope, and the phreatic line (the boundary between saturated and unsaturated zones) remains near the initial water level (29.5 m). The distribution of pore water pressure in the slope is relatively

uniform, the pore water pressure in the area above 35 m height is greater than −47.88 kPa, and the pore water pressure in the area below 35 m height increases with the depth in an approximately equal gradient, and the maximum pore water pressure is 311.22 kPa.

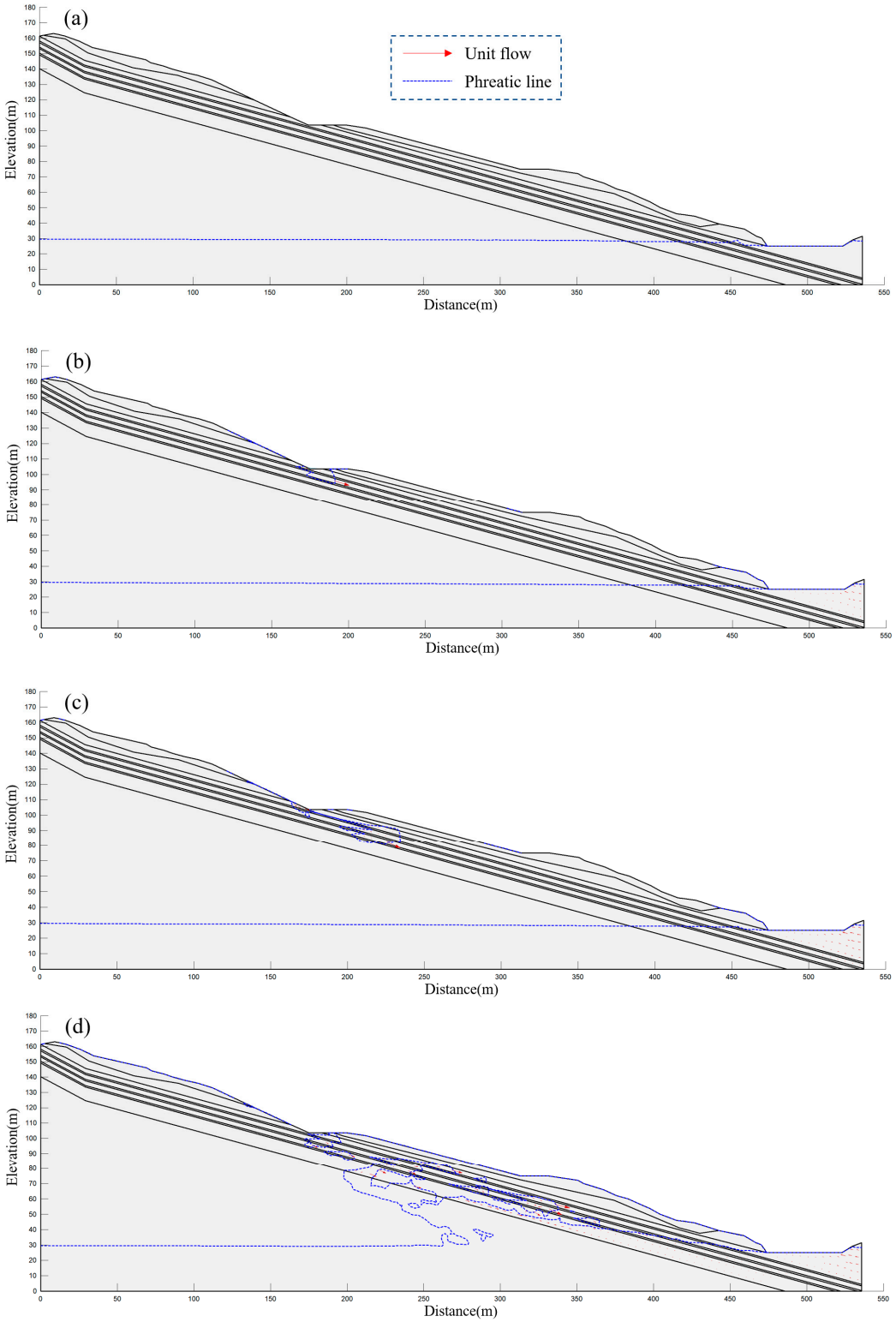


Figure 8. Unit flow and phreatic line in the highway slope: (**a**) Initial state; (**b**) 13 July; (**c**) 15 July; (**d**) 27 July.

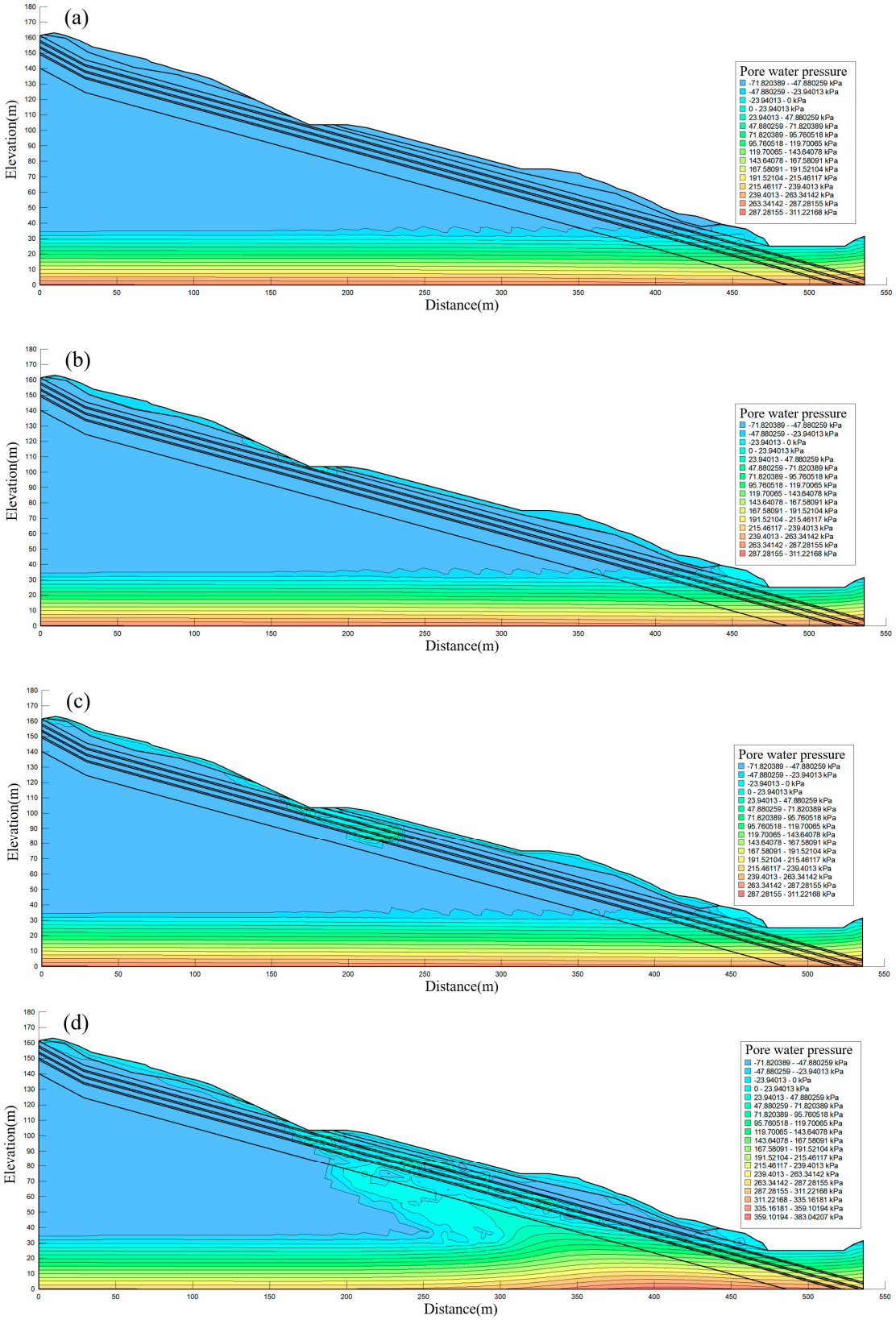


Figure 9. Pore water pressure contours for the highway slope: (**a**) Initial state; (**b**) 2 July; (**c**) 15 July; (**d**) 27 July.

The transient seepage analysis is carried out using a finite element program that divides the calculation into 27 time steps for 27 days for the seepage field at one time

step per day. Firstly, as shown in Figure 9b, the change of pore water pressure within the slope is limited on 2 July. The pore water pressure at the slope surface is in the range of −47.88 to −23.94 kPa, and the pore water pressure in the vicinity of the roadbed excavation increases to 0 kPa at the highest. This is because at the beginning of the rainfall period, the initial saturation of the slope is low, and the hydraulic conductivity of the top sub-clay and fill soils is greater than the intensity of the rainfall. Rainwater is mainly recharged by vertical infiltration, which is large and produces little flow. Then, as shown in Figure 8b, rainwater on 13 July pools in the area of the roadbed excavation and infiltrates the exposed beds of weakly weathered silty mudstone. Also, because the soft interlayer in the weakly weathered zone acts as a water barrier, rainwater enters from the rapid infiltration channel in the roadbed area and then travels down the layers. As shown in Figures 8c and 9c, rainfall continued to concentrate on infiltration on 15 July, with the phreatic line extending downward along the layers. Some of the geotechnical bodies are fully saturated, and the pore water pressure rises rapidly, with the maximum pore water pressure reaching 23.94 kPa at the roadbed.

Finally, the unit flow vectors and pore water pressures in the geotechnical body on 27 July are shown in Figures 8d and 9d, and the phreatic line extends downward along the layers to the deeper part of the slope and connects to the water table line at 30 m. At this time, the infiltrated rainwater is controlled by gravity to flow from the high side of the roadbed to the low side of the foot of the slope, forming a laminar flow movement in the pores and fissures of the rock layer, and lifting the overall groundwater level line of the slope. Phreatic water is exposed at the foot of the slope in the form of a confluence with the Danqing River, and the pore water pressure in a small area near the Danqing River is essentially stable. The geotechnical body in the roadbed–foot of the slope connection area is close to saturation, the pore water pressure rises rapidly, and local high pressure is formed inside the foot of the slope, with the maximum pore water pressure of 383.04 kPa. In summary, under highway slope conditions, the effect of heavy rainfall on the moisture distribution within the slope is significant.

4.3.2. Natural Slope Seepage Analysis

Figure 10 shows the unit flow and pore water pressure for the natural slope on 27 July, with a significant change in the way rainwater infiltrates. Different from the highway slope, in the case of the natural slope, since the roadbed area is not excavated, the strongly weathered silty mudstone and the weakly weathered silty mudstone below the surface overburden are not exposed, and the rainwater has no channel for rapid infiltration from the former roadbed area. After a small amount of the rainwater recharges the surface overburden, most of the rest of the rainwater forms surface runoff that flows from above to below to the Danqing River at the foot of the slope. The change of pore water pressure inside the slope is limited, the maximum pore water pressure remains at 311.22 kPa, and no local high pressure is formed. In summary, the effect of heavy rainfall on the internal moisture distribution of the slope is not significant under natural slope conditions.

Eight monitoring points (nodes 2341, 2347, 2344, 2343, 2342, 2349, 2346, 2348) distributed from the top to the bottom are set up at the foot of the slope, and the pore water pressure versus time curves are shown in Figure 11. At the early stages of rainfall, the pore water pressure at surface node 2341 at the foot of the highway slope and natural slope rapidly goes up to zero, reflecting the rapid saturation of the soil at the surface and the formation of surface runoff. In the middle of the rainfall, the pore water pressure at the foot of the highway slope basically remains unchanged. In the late rainfall period, the pore water pressure at the bottom of the first soft interlayer, as well as at the top and bottom of the second and third soft interlayers, in the weakly weathered zones of the highway slope rises rapidly. The pore water pressure at node 2348, which has the largest increase, grows from 130 kPa to 210 kPa. The pore water pressure at node 2344 at the top of the first soft interlayer is similarly trending upward, but by less than 10 kPa. At the end of the rainfall period, the pore water pressure difference between the top and bottom of the soft

interlayers is at its maximum. However, the pore water pressure at all nodes of the natural slope, excluding the surface node 2341, is essentially stable during all rainfall periods.

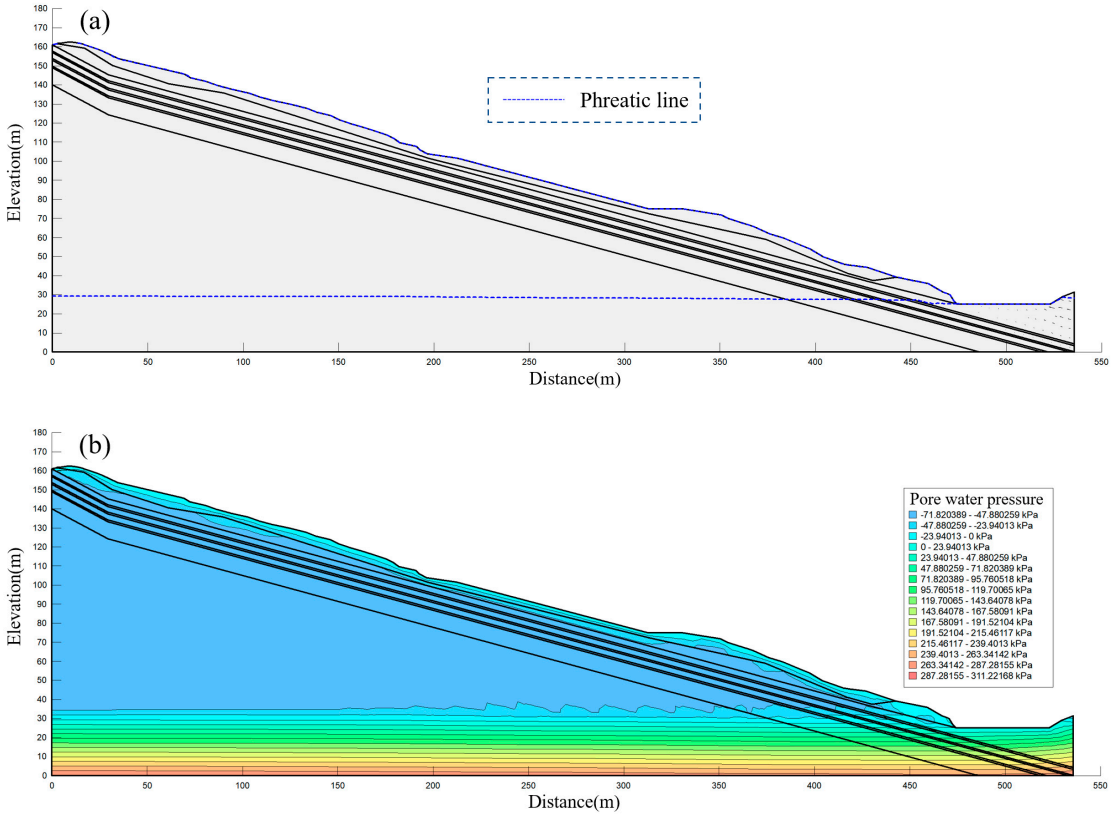


Figure 10. Seepage results for the natural slope on 27 July: (**a**) Unit flow and phreatic line; (**b**) Pore water pressure contour.

The change mechanism of pore water pressure in the highway slope is analyzed as follows: the soft interlayer in the weakly weathered zone is relatively impermeable as a water-resisting layer, and the weakly weathered silty mudstone is relatively permeable as a water-permeable layer, and the combination of the rock layers and the groundwater level reaches the conditions for the composition of typical pressurized water. Rainwater enters the slope from the fast infiltration channel in the roadbed area and then seeps downward along the permeable layer to the foot of the slope, and the infiltration and recharge of rainwater causes the pore water pressure at the bottom of the soft interlayer to increase rapidly. Although the combination of rock layers in the natural slope meets the conditions for the formation of pressurized water, the lack of water source results in constant water pressure.

4.4. Slope Stability Analysis

As shown in Figure 12, at the beginning of the rainfall, there is a phase of sudden decrease in the F_s of the highway slope, where the F_s decreases from 1.29 to 1.07. In the middle of the rainfall period, the F_s gradually decreases, and the continuous rainfall from the 10th to the 14th reduces F_s from 1.07 to 1.04, and the F_s remains essentially constant after the rain stops. In the late rainfall period, rainfall from 21 July to 22 July reduces F_s from 1.05 to 1.01. The near stopping of rain on 23 July elevates the F_s of the slope from 1.01 to 1.05 on 24 July. The deep part of the foot of the slope is located at the end of the roadbed–foot connectivity path, and there is a delayed effect in the change of F_s due to the long time it takes for rainwater to infiltrate and pass through the full path. At the end of the rainfall period, the F_s of the slope on 27 July is reduced to 0.99, with the slope in a state of instability.

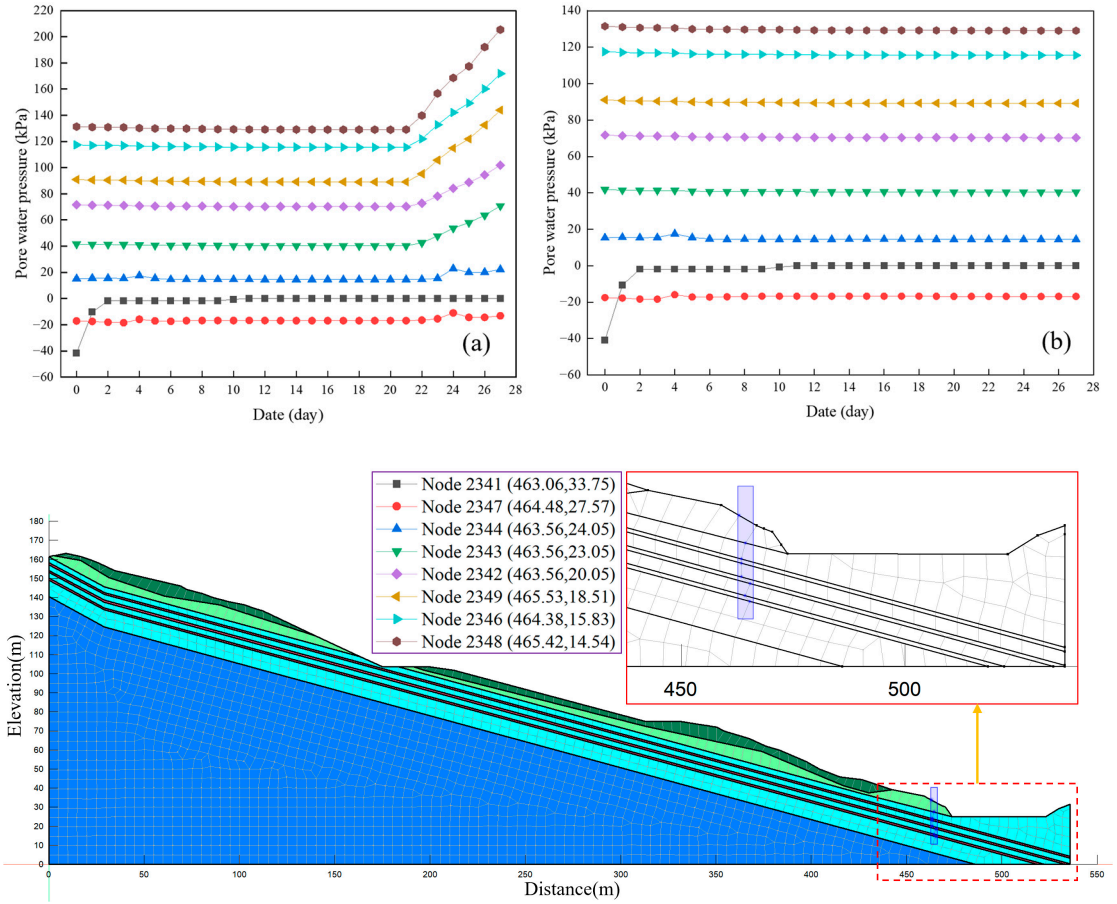


Figure 11. Pore water pressure versus time curves at monitoring points: (**a**) highway slope; (**b**) natural slope.

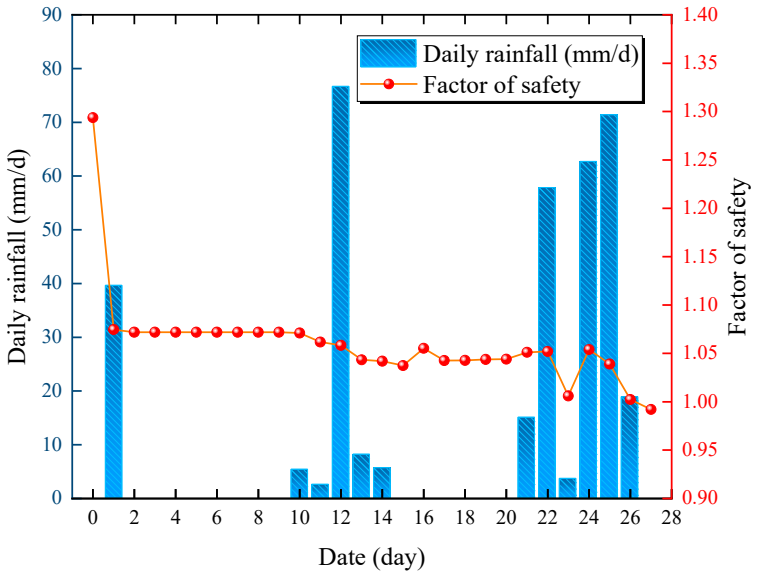


Figure 12. Factor of safety versus time curve for the highway slope.

As shown in Figure 13, after a total of 27 days of discontinuous rainfall, the F_s of the natural slope is reduced from 1.114 to 1.106, and the slope remains essentially stable. During all rainfall periods, the change in the F_s corresponds to the daily rainfall, and there is no hysteresis in the effect of rainfall on slope stability. This is because rainfall mainly

affects the saturation and pore water pressure of sub-clay and fill soils at the slope surface, and the short time required for rainfall infiltration leads to a simultaneous reduction in the shear strength of the soils.

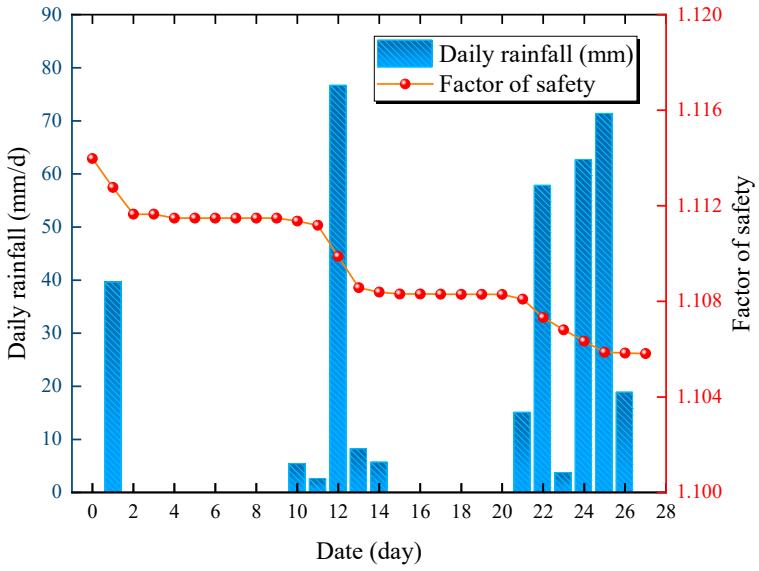


Figure 13. Factor of safety versus time curve for the natural slope.

4.5. Analysis of Highway Slope Destabilization Process

The zone maximum principal strains are shown in Figure 14. The sliding surfaces obtained from numerical simulation and actual investigation are relatively close to each other; especially in the front-edge part of the slope, they are basically the same, which reflects the reliability of the solution method based on the secondary development of FISH language considering the deterioration effect of rainwater on the geotechnical body and the buoyancy force. There are local differences between the calculated and actual sliding surface at the trailing edge of the slope, which is due to the fact that the shape of the sliding surface in the project is not only controlled by the rock layers, but also by the steeply dipping joints in the downslope direction.

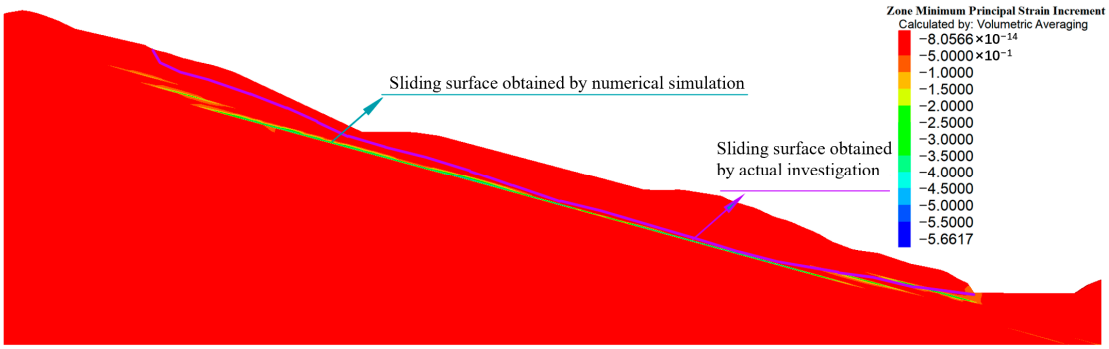


Figure 14. Maximum principal strains and sliding surfaces of the highway slope.

Combining numerical simulation and physical modeling experimental studies [29], the evolutionary process of the Zhuquedong highway landslide is visually reproduced. The slope destabilization has the following phases:

Phase 1: Flexure and uplift state, as shown in Figure 15. Gravity-driven shear deformation and differential interlayer misalignment in the rear geotechnical body produces extrusion due to blockage of the front edge, and the combined action of extrusion and water pressure causes flexural and uplift deformation of the lower rock layers. As time

progresses, the trailing edge of the slope is tensile, and the geotechnical body at the slope surface begins to slide down in small quantities.

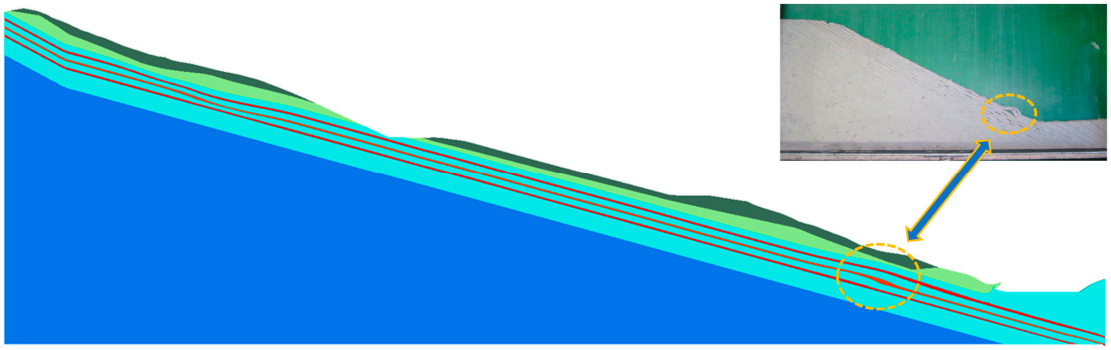


Figure 15. Highway slope flexure and uplift state.

Phase 2: Deformation exacerbation state, as shown in Figure 16. The tensile deformation at the trailing edge of the slope increases, and the middle and rear geotechnical body slips downward along the layer. The flexural and uplift deformation of the front edge of the slope is intensified and forms a fold-like bending pattern that produces localized crushing, mixing and densification of the rock at the end of the uplift. In addition, the extrusion and deformation of the rock layers toward the Danqing River in the riparian zone at the foot of the slope is intensified.

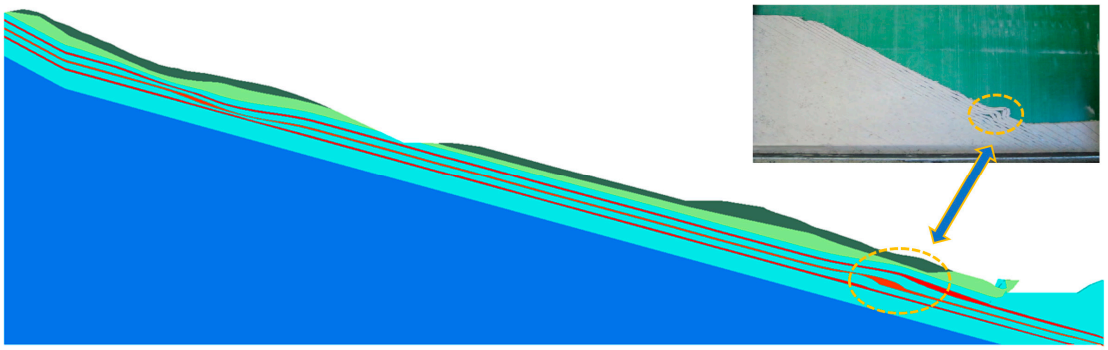


Figure 16. Highway slope deformation exacerbation state.

Phase 3: Shear failure state, as shown in Figure 17. The upper-middle silty mudstone is shear deformed and continuously pushed forward along the soft interlayers, and deformation and damage continue to accumulate in the uplift and flexural fold structure. When shear failure occurs in this area, the geotechnical body slides rapidly along this through surface, and the slope undergoes an overall destabilization failure. The actual investigation found that before the occurrence of the landslide, there was a 2–3 m high water spray near the shear outlet at the foot of the slope, which illustrated the buoyant effect of water pressure on the uplift area. When the landslide occurred, water pressure in the fissures and pore spaces was released, driving the slide mass forward and into the Danqing River. After the end of the landslide, a linearly distributed water leakage phenomenon remained on the front edge. The geological survey results showed that the landslide bed outcropping was visible at the site, the surface abrasion was developed, and its direction was consistent with the dip direction of strata. The landslide mass was mainly composed of medium-thin laminated silty mudstone sandwiched by siltstone of the Lower Cretaceous Tonglanlong Formation, which basically maintained the laminae, and the rock at the front edge was bent and elevated, and these characteristics validate the reliability of the simulation experiments.

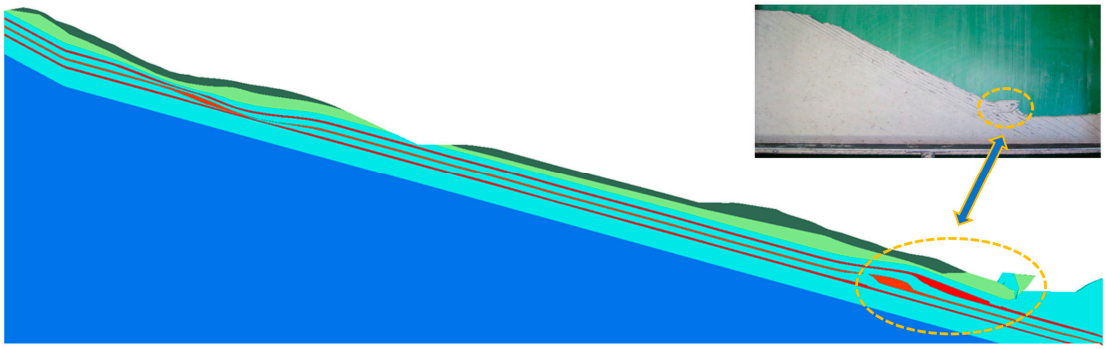


Figure 17. Highway slope shear failure state.

The destabilization processes and mechanisms of the Zhuquedong highway slope are as follows: the slope was subject to continuous heavy rainfall, and the ponding of water on the platform of the excavated section of the roadbed was more conducive to the infiltration of rainwater into the slope. Under the combined effects of gravity loading, geotechnical deterioration and water flotation, the soft interlayers and silty mudstone layers at the front edge of the slope underwent flexural and uplift deformation, which was gradually intensified, forming the uplift and flexural fold structure that produces localized crushing, mixing and densification of the rock at the end of the uplift. The tensile deformation at the trailing edge of the slope increases, and the middle and rear geotechnical bodies slip downward along the layer. As time progressed, deformation and damage accumulated, and eventually shear failure occurred in the uplift and flexural fold structure. However, in the middle and upper parts of the slope, the structural layering characteristics of the original rock were preserved, forming a typical "sliding-bending-shearing" type of instability pattern.

5. Conclusions

Through numerical simulation and theoretical analysis of large red-layered flat-dipping bedding landslides, the mechanism of rainfall infiltration and damage mechanism of the bedding slope are clarified in this study, and the following conclusions can be obtained:

(1) The effect of heavy rainfall on the water distribution inside the highway slope is significant, while F_s decreases from 1.29 to 0.99, and the slope is in a state of instability. Due to the lack of rapid rainwater infiltration channels, the effect of heavy rainfall on the water distribution inside the natural slope is not significant, while F_s decreases from 1.114 to 1.106.

(2) The sliding surfaces obtained from numerical simulation and actual investigation are relatively close to each other, which reflects the reliability of the solution method based on the secondary development of FLAC^{3D} considering the deterioration effect of rainwater on the geotechnical body and the buoyancy force.

(3) Three phases of instability and failure of the rainfall-induced red-layered bedding slope are generalized: flexure and uplift state, deformation exacerbation state and shear failure state. The slope destabilization mechanism is a typical "sliding-bending-shearing" type.

Author Contributions: Software, H.L. and L.X.; Validation, F.X. and H.H.; Formal analysis, F.X., H.H., H.L. and L.X.; Investigation, L.X.; Resources, H.H.; Writing—original draft, F.X. and H.L.; Writing—review & editing, F.X. and H.L. All authors have read and agreed to the published version of the manuscript.

Funding: This paper received funding from Postgraduate Innovative Project (2021XQLH152) of Central South University; Projects (42277175, 52204119) supported by National Natural Science Foundation of China; and Project (NRMSSHR-2022-Z08) supported by Key Laboratory of Natural Resources Monitoring and Supervision in Southern Hilly Region, Ministry of Natural Resources. The authors wish to acknowledge this support.

Institutional Review Board Statement: Not applicable.

Informed Consent Statement: Not applicable.

Data Availability Statement: The raw data supporting the conclusions of this article will be made available by the authors on request.

Conflicts of Interest: The authors declare no conflicts of interest.

References

1. Chae, B.-G.; Park, H.-J.; Catani, F.; Simoni, A.; Berti, M. Landslide prediction, monitoring and early warning: A concise review of state-of-the-art. *Geosci. J.* **2017**, *21*, 1033–1070. [CrossRef]
2. Tang, Y.; Xie, L.; Chen, Y.; Sun, S.; Zha, W.; Lin, H. Automatic recognition of slide mass and inversion analysis of landslide based on discrete element method. *Comput. Geosci.* **2023**, *176*, 105338. [CrossRef]
3. Yang, H.-T.; Bai, B.; Lin, H. Seismic magnitude calculation based on rate- and state-dependent friction law. *J. Cent. South Univ.* **2023**, *30*, 2671–2685. [CrossRef]
4. Jiang, X.; Zhu, H.; Yan, Z.; Zhang, F.; Ye, F.; Li, P.; Zhang, X.; Dai, Z.; Bai, Y.; Huang, B. A state-of-art review on development and progress of backfill grouting materials for shield tunneling. *Dev. Built Environ.* **2023**, *16*, 100250. [CrossRef]
5. Zhu, X.; Xie, L.; Tang, Y.; Chen, Y.; Hu, H.; Lu, G.; Chen, C.; Lin, H. Progressive formation of retrogressive landslide and the lateral length of instability. *Appl. Sci.* **2023**, *13*, 799. [CrossRef]
6. Kacimov, A.; Obnosov, Y.V.; Perret, J. Phreatic surface flow from a near-reservoir saturated tongue. *J. Hydrol.* **2004**, *296*, 271–281. [CrossRef]
7. Qi, G.Q.; Huang, R.Q.; Su, B.Y.; Hu, Y.J.; Zhan, M.L. Numeric simulation on rainfall infiltration on rock slope. *Chin. J. Rock Mech. Eng.* **2003**, *22*, 625–629.
8. Huat, B.B.; Ali, F.H.; Low, T. Water infiltration characteristics of unsaturated soil slope and its effect on suction and stability. *Geotech. Geol. Eng.* **2006**, *24*, 1293–1306. [CrossRef]
9. Chen, H.K.; Zhou, X.H.; Tan, L. Experimental study on the influence for rainfall characteristics to pore water pressure in landslide. *J. Chongqing Norm. Univ.* **2017**, *34*, 49–54.
10. Lian, J.F.; Luo, Q.; Jiang, L.W.; Liu, G.; Xie, T. Shallow stability analysis of soil slopes under seepage parallel to slope surface. *Chin. J. Geotech. Eng.* **2015**, *37*, 1440–1448.
11. Conte, E.; Pugliese, L.; Troncone, A. A Simple Method for Predicting Rainfall-Induced Shallow Landslides. *J. Geotech. Geoenvironmental Eng.* **2022**, *148*, 04022079. [CrossRef]
12. Liu, X.S.; Zhou, C.B. Study on discontinuous medium model for unsaturated hydro-mechanical coupling of fractured rock masses. *Chin. J. Rock Mech. Eng.* **2007**, *26*, 1485–1491.
13. Robson, E.; Milledge, D.; Utili, S.; Dattola, G. A Computationally Efficient Method to Determine the Probability of Rainfall-Triggered Cut Slope Failure Accounting for Upslope Hydrological Conditions. *Rock Mech. Rock Eng.* 2023, *ahead of print*.
14. Troncone, A.; Pugliese, L.; Parise, A.; Conte, E. A simple method to reduce mesh dependency in modelling landslides involving brittle soils. *Géotechnique Lett.* **2022**, *12*, 167–173. [CrossRef]
15. Lin, H.Z.; Yu, Y.Z.; Li, G.X.; Peng, J.B. Influence of rainfall characteristics on soil slope failure. *Chin. J. Rock Mech. Eng.* **2009**, *28*, 198–204.
16. Huang, R.Q.; Zhao, J.J.; Ju, N.P.; Deng, H.; Duan, H.P. Study on deformation mechanism and control method of bedding rock slope along tangtun expressway. *Chin. J. Rock Mech. Eng.* **2007**, *26*, 239–246.
17. Liu, H.; Bodvarsson, G. Upscaling of constitutive relations in unsaturated heterogeneous tuff matrix. *J. Hydrol.* **2003**, *276*, 198–209. [CrossRef]
18. Wu, Y.-S.; Liu, H.; Bodvarsson, G. A triple-continuum approach for modeling flow and transport processes in fractured rock. *J. Contam. Hydrol.* **2004**, *73*, 145–179. [CrossRef] [PubMed]
19. Mualem, Y. A new model for predicting the hydraulic conductivity of unsaturated porous media. *Water Resour. Res.* **1976**, *12*, 513–522. [CrossRef]
20. Fredlund, D.G.; Rahardjo, H. *Soil Mechanics for Unsaturated Soils*; John Wiley & Sons: Hoboken, NJ, USA, 1993.
21. Huang, L.; Lin, H.; Cao, P.; Zhao, Q.; Pang, Y.; Yong, W. Investigation of the Degradation Mechanism of the Tensile Mechanical Properties of Sandstone under the Corrosion of Various pH Solutions. *Materials* **2023**, *16*, 6536. [CrossRef] [PubMed]
22. Cheng, Y.M.; Lansivaara, T.; Wei, W. Two-dimensional slope stability analysis by limit equilibrium and strength reduction methods. *Comput. Geotech.* **2007**, *34*, 137–150. [CrossRef]
23. Arvin, M.R.; Zakeri, A.; Bahmani Shoorijeh, M. Using finite element strength reduction method for stability analysis of geocell-reinforced slopes. *Geotech. Geol. Eng.* **2019**, *37*, 1453–1467. [CrossRef]

24. Zhang, Y.; Xu, W.Y.; Zou, L.F.; Sun, H.K. Analysis of seepage stability of large-scale landslide under rainfall condition. *Rock Soil Mech.* **2013**, *34*, 833–841.
25. He, C.M.; Deng, X.; Fu, H.Y.; Zeng, L. Influence of Seepage Force on Stability of Coarse Grained Soil High Embankment under Rainfall Condition. *J. Highw. Transp. Res. Dev.* **2017**, *34*, 9.
26. Chen, C.Y.; Chen, H.W.; Wu, W.C. Numerical modeling of interactions of rainfall and earthquakes on slope stability analysis. *Environ. Earth Sci.* **2021**, *80*, 11. [CrossRef]
27. Zhang, X.; Yan, C.H.; Guo, S.L.; Tan, J.Z.; Xu, C.H.; Yu, L.C.; Liu, Y. Derivation of stability formula of gentle slope affected by temporary confined water. *J. Eng. Geol.* **2021**, *29*, 1507–1514.
28. Li, P.; Liu, X.; Jiang, X.; Zhang, X.; Wu, J.; Chen, P. Investigation of the first quasi-rectangular metro tunnel constructed by the 0-θ method. *Front. Struct. Civ. Eng.* **2023**, *17*, 1707–1722. [CrossRef]
29. Chen, Q.M.; Fang, Q.; Luo, G.Z.; Wang, G.W. Failure conditions and mechanism of the gentle dip bedding slopes: A case study of the Zhuquedong Landslide. *Chin. J. Geol. Hazard Control* **2020**, *31*, 18–23+32.

Disclaimer/Publisher's Note: The statements, opinions and data contained in all publications are solely those of the individual author(s) and contributor(s) and not of MDPI and/or the editor(s). MDPI and/or the editor(s) disclaim responsibility for any injury to people or property resulting from any ideas, methods, instructions or products referred to in the content.